arXiv:cond-mat/0501543v1 [cond-mat.stat-mech] 22 Jan 2005

Evolution of the structure of amorphous ice - from low-density amorphous (LDA) through high-density amorphous (HDA) to very high-density amorphous (VHDA) ice.

R. Martoňák,* D. Donadio, and M. Parrinello
Computational Science, Department of Chemistry and Applied Biosciences, ETH Zurich, USI Campus, Via Giuseppe Buffi 13, CH-6900 Lugano, Switzerland
(Dated: February 2, 2008)

We report results of molecular dynamics simulations of amorphous ice for pressures up to 22.5 kbar. The high-density amorphous ice (HDA) as prepared by pressure-induced amorphization of I_h ice at $T = 80$ K is annealed to $T = 170$ K at various pressures to allow for relaxation. Upon increase of pressure, relaxed amorphous ice undergoes a pronounced change of structure, ranging from the low-density amorphous ice (LDA) at $p = 0$, through a continuum of HDA states to the limiting very high-density amorphous ice (VHDA) regime above 10 kbar. The main part of the overall structural change takes place within the HDA megabasin, which includes a variety of structures with quite different local and medium-range order as well as network topology and spans a broad range of densities. The VHDA represents the limit to densification by adapting the hydrogen-bonded network topology, without creating interpenetrating networks. The connection between structure and metastability of various forms upon decompression and heating is studied and discussed. We also discuss the analogy with amorphous and crystalline silica. Finally, some conclusions concerning the relation between amorphous ice and supercooled water are drawn.

PACS numbers: 64.70.Kb, 61.43.Er, 02.70.Ns, 07.05.Tp

I. INTRODUCTION

Properties of amorphous solid water at low temperatures continue to attract the attention of both theory and experiment. It has been known for a long time that at least two distinct amorphous forms of ice exist. High-density amorphous ice (HDA) is prepared by compression of ordinary I_h ice to 12 kbar[1] and when recovered at ambient pressure it has a density of ~ 1.17 g/cm^3. Upon isobaric heating to 117 K, the density drops considerably and a second form is found, called low-density amorphous ice (LDA)[1] with a density ~ 0.94 g/cm^3. The transition between LDA and HDA can also be induced by pressure[2,3]. Interest in this system is enhanced by the possible existence of a second critical point in water, proposed originally in Ref.[4] and later elaborated in several variants (Refs.[5],[6],[7]). According to this hypothesis, in the deeply supercooled region a second critical point should exist, below which two kinds of water, high-density liquid (HDL) and low-density liquid (LDL) are separated via a first-order phase transition. Experimentally, however, it has not yet been possible to access the deeply supercooled region and directly investigate its properties. In the lack of direct evidence, the existence of two different amorphous forms of ice has been used as an indirect support for this hypothesis, assuming that HDA and LDA, apparently separated by a sharp transition, are simply glassy forms of HDL and LDL[8].

Recently several new experimental results[9,10,11,12,13,14,15,16] raised new questions about the nature of amorphous ices as well as about their relation to the speculated second critical point of water. A new amorphous form of ice has been reported[9], prepared by heating HDA under pressure of 11 kbar to $T \sim 170$ K and cooling it back to $T = 80$ K; when recovered at ambient pressure it has a density of ~ 1.25 g/cm^3. It has been called very high-density amorphous ice (VHDA) and characterized experimentally by neutron diffraction[11]. More detailed structural measurements of VHDA ice were performed very recently[17] and showed that the radial distribution function (RDF) of VHDA is in fact more structured than that of HDA and LDA, revealing the presence of an enhanced medium-range order. Other experiments[12,13,14,16] focused on the HDA-LDA transition induced by heating at ambient or low pressure. In Ref.[12] it was shown that by heating HDA to temperatures intermediate between 80 K and 110 K the sample can be trapped in an apparent continuum of metastable structures between HDA and LDA. This suggests that there might be no sharp transition between the two forms. In Ref.[13] the kinetics of the HDA to LDA transition was studied; this revealed three stages of the transformation, consisting of the annealing of HDA, followed by an accelerated transition to the LDA form and subsequent annealing of the LDA. The experiment in Ref.[15], while also finding a continuum of HDA states, observed also a propagation of the LDA-HDA interface, thus providing evidence in favor of a sharp transition between the two forms. Possible implications of the new experiments have been discussed[16,18,19]. Several review papers on amorphous and supercooled water have also appeared recently, see Refs.[20],[21],[22].

Simulations can complement the experiment by providing access to shorter time scales, not easily accessed in experiment. At the same time they can provide detailed structural information which might not be easily extracted from the experimental data. The basic phenomenology of amorphous ices has been reproduced in earlier works[8,23,24]. New simulations have also been performed recently[25],[26],[27],[28],[29],[30].

Here we present the results of extensive constant-pressure MD simulations of amorphous ice at temperatures 80 - 170 K and pressures up to 22.5 kbar. We focus on the structure of the annealed form of amorphous ice and study its evolution under increasing pressure. We identify the LDA and HDA regimes, possibly separated by a transition. VHDA on the other hand does not appear to be a new phase, but rather a particular high-pressure regime of HDA. In particular, we suggest that both new phenomena, the VHDA and the continuum of metastable HDA densities at ambient pressure, originate from the relationship between the density and the topology of the hydrogen-bonded network of the HDA phase. A preliminary account of this work has already been published in Ref.[31]. Here we present a more detailed account of the results as well as new simulations and new analysis. The paper is organized as follows. In section II we present the model and details of our simulation technique. In section III we present our results. First we describe the protocol used to prepare various forms of amorphous ice and then discuss in detail their properties, comparing with experiment as well as with other simulations. In section IV we draw an analogy of another important tetrahedrally-bonded system, amorphous silica. Finally, in the last section V we summarize our findings and draw some conclusions concerning the relation between amorphous ice and supercooled water.

II. MODEL AND TECHNIQUE

Our tool is constant-pressure molecular dynamics (MD) simulation. We employed the GROMACS code[32] using the Parrinello-Rahman constant-pressure MD[33], the Berendsen thermostat[34] and a time step of 2 fs. Electrostatic interactions were treated by the particle-mesh Ewald method[35]. An initial proton-disordered configuration of I_h ice with 360 H_2O molecules and zero dipole moment in an orthorhombic box was prepared using the Monte Carlo procedure of Ref.[36].

The interaction between water molecules was described by the classical TIP4P model[37]. In previous simulations this was found to reproduce well the transitions I_h – HDA and LDA – HDA, both qualitatively and quantitatively[8,23,24]. Although it is known to systematically overestimate the experimental ice densities by about 2 %, the TIP4P model has recently been shown to be capable of predicting qualitatively correctly the entire phase diagram of water[38].

III. RESULTS AND DISCUSSION

A. Preparation and annealing of amorphous ice

First we shall describe the simulation protocol that we applied. We started by compressing the ice I_h at $T = 80$ K, increasing the pressure in steps of 1.5 kbar. At 13.5 kbar a sharp transition occurs and the density increases by almost 30 % to 1.37 g/cm^3 (Fig.1). The sample was then further compressed at $T = 80$ K to 22.5 kbar and from 15 kbar decompressed to $p = 0$. This particular HDA form obtained by pressure-induced amorphization of I_h ice at $T = 80$ K and subsequent compression or decompression, without any thermal treatment, will be in the following denoted by HDA' (as-prepared HDA phase). During decompression the HDA' density gradually decreased and at $p = 0$ reached the value of 1.19 g/cm^3, close to the HDA experimental value of 1.17 g/cm^3[31]. The radial distribution function (RDF) of HDA' at $p = 0$ is shown in Fig.2; it has a broad second peak between 3.3 and 4.6 Å, very similar to that of HDA at $p = 0$[10]. Inspired by the experiments[9] that led to the discovery of the VHDA we decided to anneal the HDA' phase at each intermediate pressure between 22.5 kbar and zero (a similar treatment was applied in Ref.[9] at $p = 8.4, 11$ and 19 kbar) in order to search for possible new structures. Annealing was performed by heating up to $T = 170$ K and subsequent cooling down to 80 K; the temperature was always changed in steps of 10 K. The phase obtained in this way will be called relaxed phase (RP). We note here that in Ref.[39] a slow molecular diffusion was observed in the MD simulation of the TIP4P model at $T = 173$ K; therefore at 170 K it should be possible to equilibrate the system within accessible simulation times. While in experiments a HDA' sample heated at an arbitrary pressure might recrystallize[8,18,40], in the time scale of a simulation this is not likely to happen. We are therefore restricted to exploring the (metastable) disordered structures. In order to check the metastability of the RP phase upon decompression, the RP prepared at each pressure was finally decompressed at $T = 80$ K down to $p = 0$, decreasing the pressure in steps of 1.5 kbar.

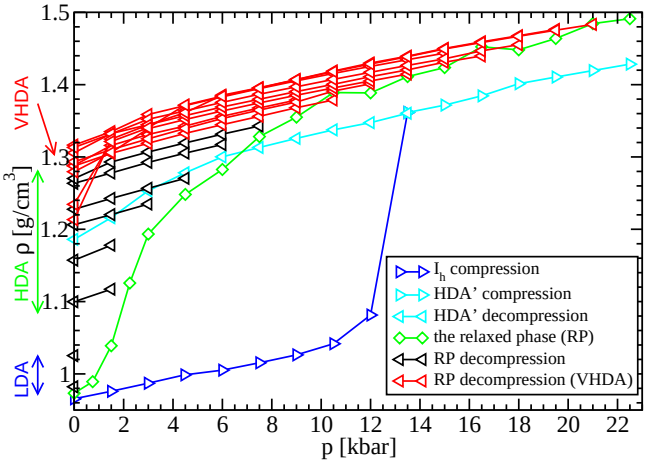

FIG. 1: Density vs. pressure dependence at $T = 80$ K for the various amorphous phases during compression/decompression. The triangles point in the direction of pressure change, the lines are just a guide for the eye.

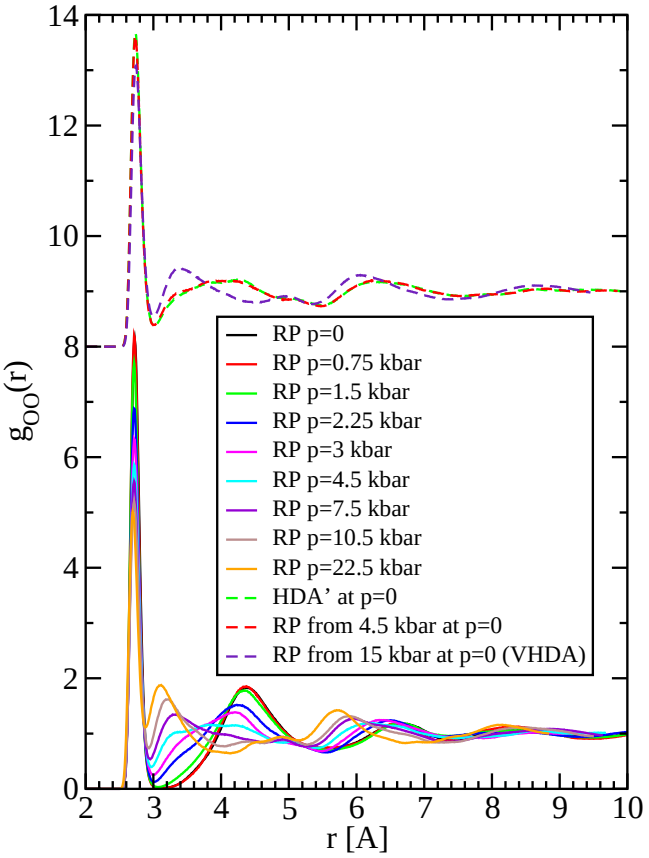

FIG. 2: Oxygen – oxygen radial distribution function of various amorphous phases at $T = 80$ K and $p = 0 - 22.5$ kbar. The curves in the upper part of the figure have been shifted by 8 for clarity.

After each change of pressure or temperature the system was equilibrated for 5 ns and observable quantities were averaged over 0.5 ns. An additional equilibration for 25 – 50 ns was performed during the annealing at the highest temperature of $T = 170$ K. We stress here that the long equilibration times are indeed necessary in order to allow the system to undergo structural changes; e.g at pressure $p = 0.75$ kbar the equilibration of the system at $T = 170$ K takes about 20 ns. A comprehensive summary of the density vs. pressure dependence of I_h, HDA', RP and decompressed RP phases at $T = 80$ K is presented in Fig.1 and will be discussed in detail in the next section.

In Fig.3 we show the relaxation of the density during annealing of the HDA' ice at $p = 16.5$ kbar to $T = 170$ K. It can be seen that upon annealing at 90 and 100 K the density grows while between 110 and 130 K the sample undergoes a thermal expansion. At 140 K and 150 K the density grows further but no substantial change is observed above $T = 150$ K.

We have verified that the enthalpy of the relaxed phase is lower than that of HDA' ice at any pressure (Fig.4). Assuming that the entropy contribution to the Gibbs potential can be neglected at $T = 80$ K (and entropy differences between amorphous phases are anyway expected to

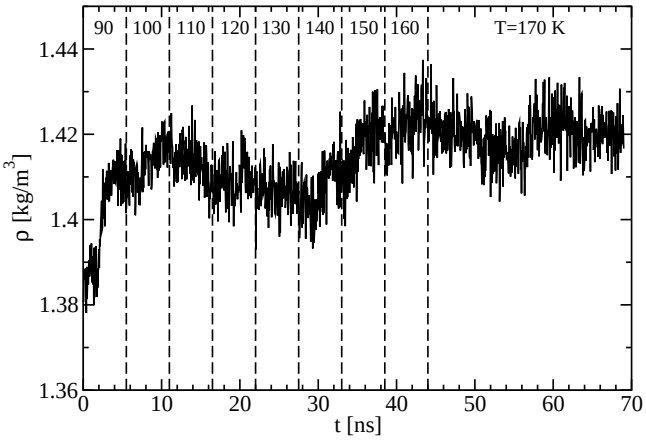

FIG. 3: Time dependence of the density during annealing of the HDA' ice at $p = 16.5$ kbar to $T = 170$ K. Points where the temperature is increased by 10 K are marked by vertical dashed lines. The temperature (in K) during each time interval is shown in the top part of the figure.

be small[41]) this demonstrates that upon annealing at any pressure HDA' ice irreversibly relaxes to a state with a lower free energy. This a posteriori justifies the necessity of annealing in order to reach a metastable equilibrium corresponding at each pressure to a well-defined thermodynamic phase. We note that the lowest difference between the enthalpy of the HDA' phase and that of the RP is found at $p = 4.5$ kbar, suggesting that at the latter pressure HDA' is closest to its corresponding relaxed amorphous form (see also next subsection).

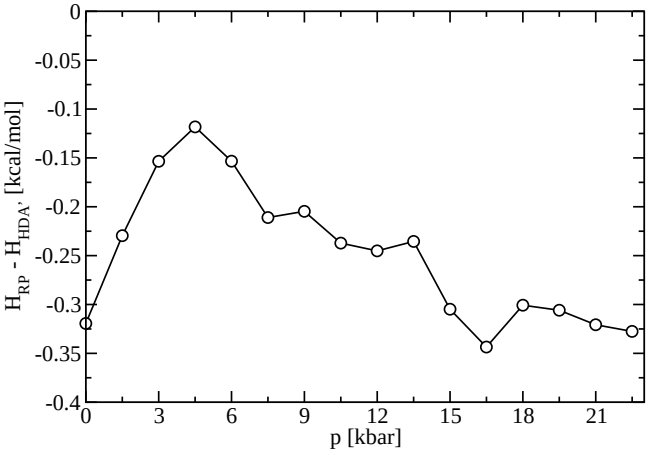

FIG. 4: Decrease of enthalpy upon annealing: difference between the enthalpy of the RP phase and that of the HDA' phase at T=80 K.

B. Evolution of the RP with increasing pressure

In this section we analyze the properties of the RP and their dependence on pressure, with the focus on struc-

ture. The density vs. pressure dependence of the RP (Fig. 1) can be considered as the equation of state of amorphous ice. We note first that the HDA' and RP curves cross at about 7 kbar; for lower pressure annealing results in lower density while for higher pressures the system densifies.

At $p = 0$ the density after annealing reaches a value of 0.97 g/cm^3, which agrees well with the experimental LDA value of 0.94 g/cm^3. The remarkable feature of the RP curve is the narrow region between 1.5 and 2.25 kbar where the density increases by about 9 %, from 1.04 g/cm^3 to 1.13 g/cm^3. Upon further increase of pressure the density grows fast and reaches at $p = 3$ kbar the value of 1.19 g/cm^3. Beyond that point the density growth slows down progressively and at the highest pressure of 22.5 kbar the density reaches a value of 1.49 g/cm^3.

The O-O RDF's of RP at different pressures are shown in Fig.2. We also calculated the O-H RDF (not shown) for RP at $p = 0, 2.25, 6$ and 15 kbar. Integrating between 1.5 and 2.25 Å we found at all pressures a coordination number of 2, indicating a fully hydrogen-bonded network. In order to characterize the evolution of the network topology we calculated the ring statistics for RP at all pressures. This reveals information on medium-range order that otherwise might not be easily extracted from the RDF[42,43]. We applied the ring counting algorithm[44] using the criterion from Ref.[45] to identify the hydrogen bonds (we used for the O-O distance a cutoff parameter of $r_{cut} = 3.05$ Å and a tolerance of $\Delta = 0.2$ Å). Our aim is to draw qualitative conclusions, so we did not try to bring down the statistical error by repeating several times the quench from 170 K to 80 K and averaging over the resulting structures. We now discuss the evolution of the RP at increasing pressure in terms of RDF and network ring statistics (Fig.5) and show that there are 3 distinct regimes.

The RDF of the RP at $p = 0$ (Fig.2) exhibits at $r = 3.1$ Å a very deep minimum between the first and second shell and a well-defined second shell peak at $r = 4.4$ Å, very similar to that found experimentally for LDA in Ref.[46]. The phase thus coincides with the LDA as expected. The same is true at 0.75 kbar at a density of 0.99 g/cm^3, where the RDF within the second peak is practically indistinguishable from the one at $p = 0$, and only beyond 5 Å can small differences be seen. At 1.5 kbar the density increases to 1.04 g/cm^3 while the RDF becomes slightly different from that of LDA at $p = 0$; the very deep minimum between the first and second shell is still present. At all these pressures the network is dominated by 6-membered rings.

The properties of the RP at $p = 2.25$ kbar are rather different, correlating with the sharp increase of density. The second shell peak of the RDF drops and shifts to lower r and at the same time the RDF grows substantially in the region around $r = 3.3$ Å, revealing the presence of interstitial molecules[10]. A dramatic change is seen in the ring statistics: the number of 6-membered rings now starts to drop and at the same time the number of 8-membered rings grows fast. This behavior is compatible with a transition from LDA to HDA occurring between 1.5 and 2.25 kbar. Around $p = 4.5$ kbar the RDF develops a broad second peak between 3.2 and 4.4 Å, similar to that of HDA' at $p = 0$ (Fig.2). This agrees with the observation based on the enthalpy difference and shows that the HDA' is indeed closest to the RP at this pressure. Approaching $p \sim 10$ kbar the ring statistics are definitely dominated by 8 and 9-membered rings; the network has thus undergone a substantial reconstruction (see also section IV). For $p > 10$ kbar, the ring statistics almost stabilize, revealing that the reconstruction of the network is practically completed; at the same time the density growth slows down further and the compressibility approaches that of ice I$_h$. This indicates that the increase of density due to the more efficient packing of the molecules has at $p \sim 10$ kbar reached its limit at the value of $\rho_{lim} \sim 1.39$ g/cm^3, and further compression proceeds mainly by elastic compression. In this limiting regime the RDF develops a pronounced second peak at $r = 3.2$ Å (Fig.2) while the original second shell peak at $r = 4.4$ Å disappears completely. In the subsection III E we will identify this regime with the VHDA form.

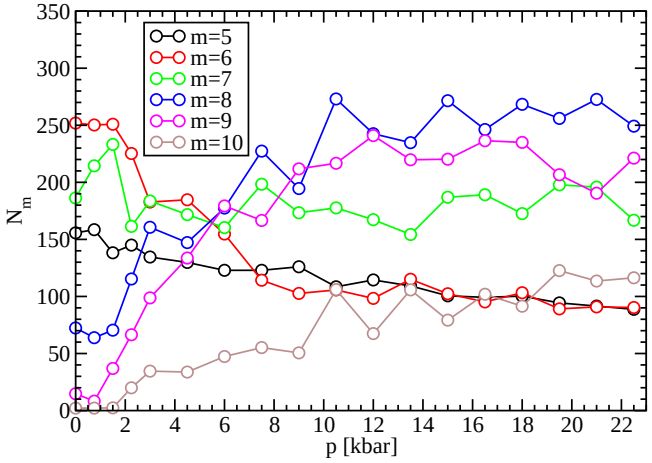

FIG. 5: Number of n-membered network rings in the RP as a function of pressure at $T = 80$ K and $p = 0 - 22.5$ kbar.

The above analysis provides quite a clear picture of the evolution of the network topology when going from LDA to VHDA. Concerning this point, rather contradictory opinions have been presented in the literature, based on the indirect information provided by the detailed analysis of radial and spatial distribution functions obtained from diffraction experiments and the empirical potential structure refinement procedure[47]. First we note that there is no sign of any discontinuity upon evolution of the HDA phase into the limiting VHDA regime. In Ref.[11] it was speculated that there is no need to postulate any significant reorganization of the network structure in moving between HDA and VHDA and that they appear topologically isomorphous. Our results, however, show clearly that the evolution of HDA between 2.25 kbar

and 10 kbar must inevitably involve a substantial reconstruction of the network. On the other hand, in Ref.[10] it was suggested that HDA' under pressure shows some characteristics of interpenetrating networks, similar to those of high-pressure crystalline ices VII and VIII. We checked this feature in the RP up to the highest pressure investigated, using the following algorithm. Starting from each molecule we considered a sphere with radius $r_{cut} = 5$ Å and tested whether the molecules within the sphere were connected to the central one by a path containing no more than 4 hydrogen bonds. We found that practically all molecules fulfilled this criterion; this is clearly incompatible with the presence of interpenetrating networks[31]. The VHDA structure can therefore be considered as the upper limit to efficient amorphous packing of the molecules without creating interpenetrating networks, as suggested in Ref.[11]. Still, it is an interesting question whether amorphous ice with interpenetrating networks can exist. Very recently, a study of VHDA was performed[48] in the region of densities ranging up to 1.9 g/cm^3, thus much higher than those studied here. Based on the analysis of bond angle distributions, they showed that VHDA at very high densities approaches a disordered close-packed structure, with local order more similar to the fcc/hcp than to the bcc crystal. From this they concluded that VHDA does not represent a disordered version of ice VII and therefore does not have interpenetrating networks. The algorithm applied here in fact provides direct evidence. We have also generated a sample of the RP at $p = 42$ kbar, with density $\rho = 1.61$ g/cm^3, and found that the ring statistics were practically equal to the average of the RP in the interval 10 - 22.5 kbar. This shows that the network topology stabilizes already for densities $\rho > \rho_{\rm lim} \sim 1.39$ g/cm^3, although the local order converges only at much higher densities.

C. Analysis of the shape of the rings

In order to obtain a deeper insight into the structural response to pressure of the RP in the three regimes (LDA, HDA, VHDA), we also performed a more detailed analysis of the network structure, separating the contributions coming from different rings.

The shape of the rings has been characterized through the eigenvalues of the inertia tensor. Given the three eigenvalues I_1, I_2 and I_3, sorted by increasing magnitude, we define an elongation parameter ϵ as $\epsilon = (I_2 - I_1)/I_3$ and the asphericity (α) as the root mean square deviation of I_i normalized to I_3. According to the definitions, ϵ can vary from 0, for a circular ring or a sphere, to 1 for a linear arrangement, while α is zero for a sphere, 0.236 for a circular ring and 0.58 for a linear arrangement. The distribution of α for all the rings considered is peaked around ~ 0.2 at $p = 0$. Increasing the pressure increases the spreads of the distribution and shifts the peak toward higher α. The tail of the distribution never extends below 0.15, which means that the rings are mainly planar structures.

The probability distribution of the elongation parameter provides a clear indication of the evolution of the shape of different rings as a function of the pressure. In HDA at $p = 2.25$ kbar (Fig.6a) the P(ϵ) shows that the water molecules in five and six-membered rings arrange themselves in circular rings. The larger the ring the broader the distribution, indicating that larger rings can arrange into elongated structures without paying too much in terms of strain energy. P(ϵ) at different pressures for six and nine-membered rings are shown in Fig.6 panels (b) and (c), respectively. Six and nine-membered rings, the quantity of which is most affected by pressure-induced phase transitions, are shown as representative of the behavior of small and large rings under pressure, respectively. At low pressures (up to 2.25 kbar) the shape of the small rings (Fig.6b) remains unchanged but when the transition to HDA occurs their number rapidly decreases, and elongated large eight and nine-membered rings are formed. In fact, already at $p = 1.5$ kbar the main peak of the $P(\epsilon)$ of nine-membered rings (Fig.6c) shifts from 0.1 to 0.48. The broad $P(\epsilon)$'s of large rings at higher pressures show that such rings can easily adapt to any shape so as to achieve a more efficient compaction. In the HDA region the morphology of small rings evolves toward more elongated shapes and their amount decreases continuously. When the onset pressure for the VHDA regime is reached, the topology of the amorphous network stops changing and also the $P(\epsilon)$'s stabilize. The residual small rings in VHDA are arranged into elongated structures (the P(ϵ) is peaked at 0.4), whereas the $P(\epsilon)$ of the nine-membered rings has no sharp peaks. At this regime the response to further compression consists in the deformation of short-range structural features, such as the bond angle distributions, as no more important rebonding is induced by increasing the pressure up to 42 kbar.

We define a ring-restricted radial distribution function n-rRDF(r) as the probability of finding two atoms at a distance r within the same n-membered ring. This quantity allows us both to recognize the separate contribution of different rings to the $g(r)$ and to characterize the response of different rings to compression. In Fig.7 the oxygen-oxygen n-rRDF(r) at different pressures are shown for six and nine-membered rings. The position of the first peak of both rRDF's is unaffected by compression up to 15 kbar and even a compression to 42 kbar induces a shift as small as 0.04 Å. Low pressures up to 2.25 kbar do not affect significantly the 6-rRDF, whereas in the same range of pressures nine-membered rings already provide a sizable contribution to the interstitial region between the first and the second peak of the $g(r)$. In the region of stability of the HDA (6 kbar) six-membered rings are strained and contribute to the interstitial region of the $g(r)$ through a broadening and a shifting to the left of the second peak. On the other hand the second peak of the 9-rRDF(r) spreads partly in the

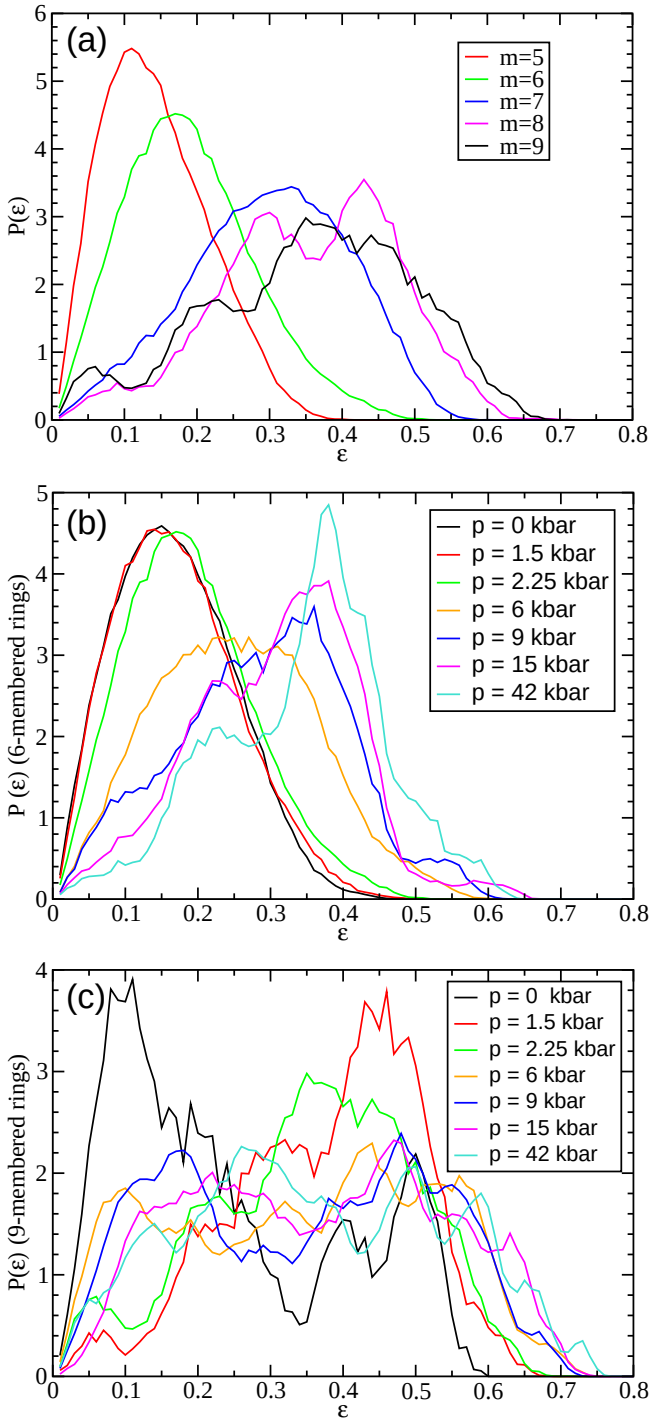

FIG. 6: (a) Probability distribution of the elongation parameter of the rings in HDA at 2.25 kbar. (b) and (c) P(ϵ) at several pressures from LDA to VHDA for six and nine-membered rings, respectively. We note that all the curves are normalized to one and therefore do not reflect the change of the total number of rings with a given size.

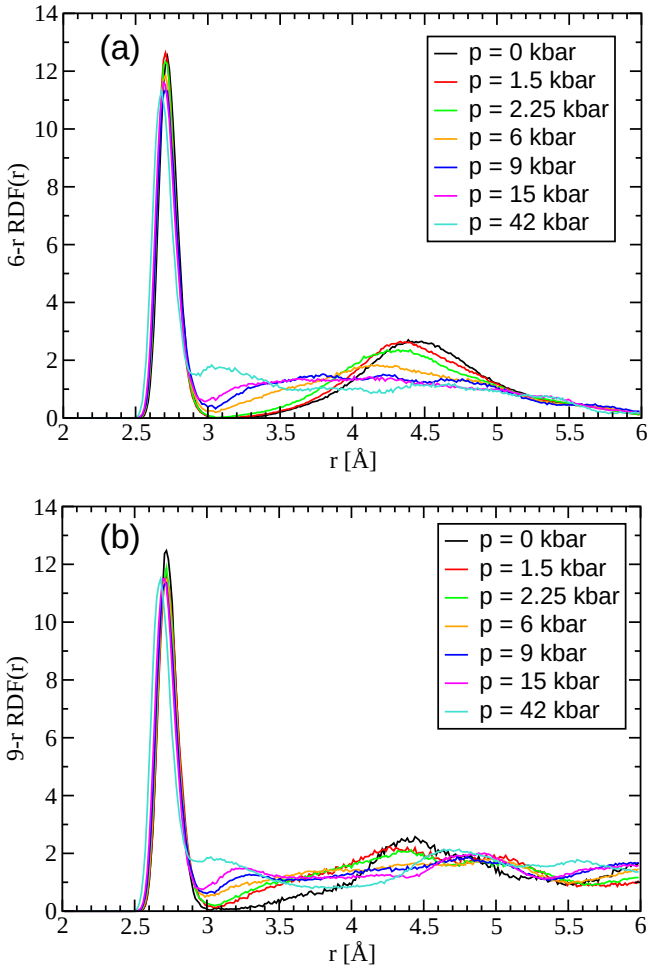

FIG. 7: Ring-restricted radial distribution function at several pressures for six (a) and nine-membered (b) rings.

interstitial region and gives rise to a shallow peak at 4.9 Å. Such a peak becomes more pronounced as the pressure increases and is a feature of VHDA[17]. It is worth noting that even at 42 kbar the six-membered rings do not provide a sharp contribution to this feature. We note that the rRDFs fully account for the interstitial peak in the $g(r)$ of VHDA, showing that this peak originates from contributions within the same ring. This constitutes independent evidence that there is no formation of interpenetrating networks.

D. Transition LDA-HDA

The question of whether there is indeed a transition between LDA and HDA and, if so, what its character is, is of great importance. From the ring statistics shown in Fig.5 it can be seen that the response of the number of rings to the applied pressure is rather different in the regions below 1.5 and above 2.25 kbar. Because of the limited accuracy of the ring statistics calculated in the frozen states, we can conclude that this behavior is

compatible with the existence of a phase transition as required by the second critical point scenario[4].

In order to determine whether the density of the RP changes discontinuously between 1.5 and 2.25 kbar, we performed at $T = 170$ K also a ~ 30 ns simulation at an intermediate pressure of 1.875 kbar. We did not observe any metastability or hysteresis effects but instead rather large and slow density fluctuations. Since our system is relatively small, such behavior is compatible with a weak first order transition, occurring just below the critical temperature, where the system oscillates over a low barrier between two states. In principle it is, however, also possible that the change of density with pressure is genuinely continuous, with a highly compressible region between 1.5 and 2.25 kbar. In order to shed more light on this important issue, it would be necessary to perform simulations with larger systems, including several system sizes, and apply standard finite-size scaling techniques[49]. It might also be useful to perform free energy calculations, e.g. umbrella sampling, with a suitable order parameter, similar to that performed in Ref.[50]. Both techniques would, however, require considerable CPU resources to achieve a good equilibration and sampling, since in the interesting region the free energy surface is very rough, resulting in very long autocorrelation times.

E. Decompression of RP to $p = 0$

Most experimental data on amorphous ices have been gathered on samples decompressed to ambient pressure. To our knowledge, there are no experimental data for the RP under pressure to which we could directly compare our results of the subsection III B. We discuss now the interesting behavior of the RP upon decompression.

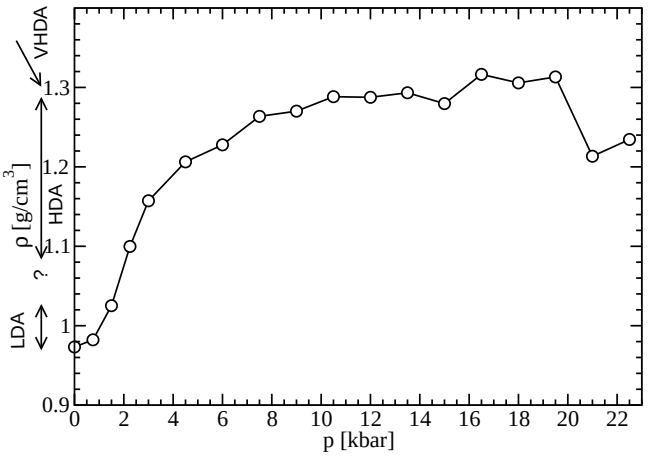

FIG. 8: Density of the RP after decompression at $T = 80$ K from pressure p.

The density of the LDA phase from 0.75 kbar relaxes at $p = 0$ to $\rho = 0.98$ g/cm^3, very close to the $\rho = 0.97$ g/cm^3 of LDA prepared at $p = 0$. The LDA phase from 1.5 kbar on the other hand reaches at $p = 0$ a somewhat higher value of $\rho = 1.025$ g/cm^3, suggesting the possibility that at $T = 80$ K and $p = 0$ there might not be a unique structure of the LDA (in agreement with Refs.[26],[13]) and this phase can actually span a narrow density interval. In the pressure interval $p = 2.25 - 10$ kbar, all decompression curves are roughly parallel (Fig.1) and the faster growing RP density results upon decompression in an increasing density at $p = 0$, spanning the interval from 1.10 to 1.26 g/cm^3. The picture changes remarkably for $p > 10$ kbar. Here, the slope of the RP curve becomes close to that of the decompression curves which lie close to each other and initially almost follow the RP curve. Decompression from almost all pressures results at $p = 0$ in a narrow interval of densities around $\rho_{VHDA} \sim 1.29$ g/cm^3, corresponding to the decompression from the limiting density ρ_{lim}. For convenience, in Fig.8 we show the dependence of the final $p = 0$ density on the original pressure p at which the RP was prepared, where the saturation can be clearly seen. This agrees very well with the observation in Ref.[9] where the samples annealed at 11 and 19 kbar reached upon decompression the same VHDA density of 1.25 g/cm^3; in fact, this was the reason why VHDA was originally suspected to represent a new thermodynamic phase. The RDF of RP decompressed from 15 kbar (Fig.2) is clearly similar to that of VHDA recovered at $p = 0$ in experiment[11], showing the presence of the distinct peak at $r = 3.37$ Å, very close to the first shell peak. This allows us to identify this form as VHDA. The spectrum of metastable states at $p = 0$ (Fig.8) is thus compatible with the existence of a narrow LDA region and a broad continuum of metastable HDA states with a density below that of VHDA (as found experimentally in Ref.[15]). We note that the density spectrum of the HDA states extends both above and below that of the HDA', and there is no reason to consider HDA' as a particular state representative of the HDA phase. While the LDA states might be separated from the HDA ones by a gap, it must certainly be much smaller than the density difference between LDA and HDA' at $p = 0$.

We now suggest an explanation for the existence of an upper limit ρ_{VHDA} to the density of metastable HDA at $T = 80$ K and $p = 0$. In the HDA phase with $\rho < \rho_{lim}$, the system with increasing pressure achieves a better packing of molecules due to network reconstruction. This must involve the breaking and remaking of bonds, which at any density requires crossing a free energy barrier, and is only possible due to the annealing at higher temperature, in our case 170 K. During cooling to 80 K, the network topology becomes frozen. Upon subsequent decompression at 80 K, the barriers cannot be crossed and therefore the system cannot relax to a lower density via reconstruction of the network. This is illustrated in Fig.9 where the evolution of the ring statistics upon decompression of the RP from $p = 13.5$ kbar is shown; it can be seen that no pronounced change in the network topology occurs. The largest change is seen in the number of 9 and 8-membered rings, which decrease by about 20 % and

9%, respectively, while the number of other rings stays practically constant. The decompression thus proceeds dominantly via relaxation of the elastic compression and that is why the HDA states with $\rho < \rho_{lim}$, which have a variety of different topologies, relax elastically to different states, spanning a range in density. On the other hand, all HDA states with $\rho > \rho_{lim}$, which have almost the same network topology, relax upon decompression to the same density ρ_{VHDA}. This accounts for the behavior observed in Ref.[9], with no need to postulate VHDA to be a new phase, and is also consistent with the fact that we did not observe any discontinuity during the evolution from HDA to VHDA. The origin of the behavior of VHDA upon decompression therefore appears to be kinetic rather than thermodynamic.

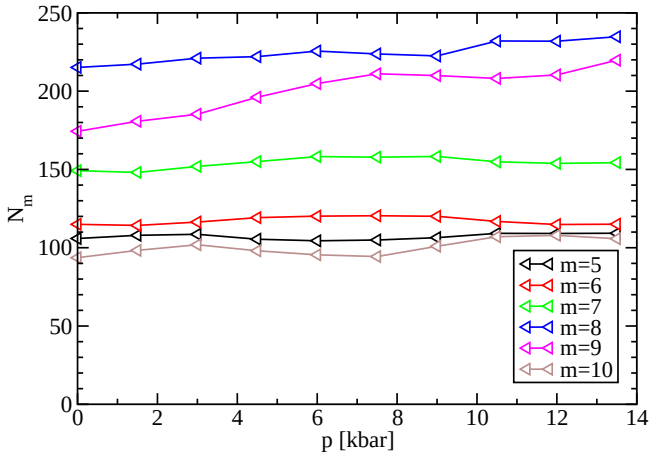

FIG. 9: Ring statistics during the decompression of RP at $T = 80$ K from $p = 13.5$ kbar to zero.

The two points from the highest pressures of 21 and 22.5 kbar reach upon decompression a lower density, 1.21 and 1.23 g/cm^3, respectively. We believe that this is related to the fact that our decompression is performed too fast, resulting in excessive elastic energy at $p = 0$. This may, in turn, allow some barriers to be crossed and enable a transition to a density $\rho < \rho_{VHDA}$.

We comment now on the experiments[12,14], where HDA' was heated to intermediate temperatures between 80 and 120 K and at each temperature annealed for several hours. On this time scale every increase of temperature resulted in an initial slow drop of the density which afterwards gradually stabilized; an additional drop of the density could be observed only by further increase of temperature. This behavior clearly points to the fact that as the HDA phase approaches its low density limit, the barriers increase and can be overcome only at a higher temperature. Our picture of the structural evolution of the HDA phase is compatible with these experimental findings. It is plausible to assume that the height of the barriers is correlated to the amount of network reconstruction necessary to change the volume, and is therefore related to the pressure derivatives of the number of rings. As shown in section III B, the reconstruction of the RP upon increasing pressure is most dramatic at the low density limit of the HDA spectrum, and with increasing density becomes gradually less pronounced, until it practically vanishes for $\rho > \rho_{lim}$. We explicitly checked the degree of metastability of HDA forms with different densities (RP decompressed from several different pressures) by heating at $p = 0$; the results are shown in Fig.10. The temperature was increased in steps of 10 K, spending 5.5 ns at each temperature, and we note that also here it would be useful to perform the heating several times and average in order to improve the statistical error. Nevertheless, it can be clearly seen that the most stable structure under heating is actually the lowest density HDA (RP decompressed from 2.25 kbar) which undergoes only a small drop in density up to 130 K. With increasing initial density the samples start to relax at lower temperature, which confirms the above relation between the network topology and barriers. It is also seen that HDA' is the least stable of all the samples, as may be expected for an insufficiently equilibrated phase possessing an excess free energy. We stress that at $T = 170$ K all curves reach practically the same density, lower than 0.99 g/cm^3, which also agrees with the experimental finding in Refs.[9,11] that VHDA upon heating converts to LDA. This is different from what found in Ref.[28] where it was argued that VHDA upon heating converts to a different form of LDA, with a higher density of about 1.04 g/cm^3.

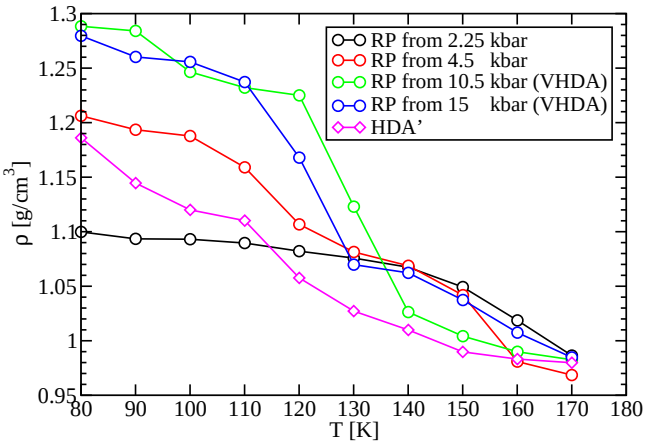

FIG. 10: Density as a function of temperature during heating of various decompressed RP phases as well as HDA' at $p = 0$.

In Ref.[28] various HDA forms were prepared by an alternative procedure, consisting of the pressure-induced amorphization of cubic ice at different temperatures ranging from 50 to 300 K. It was concluded that the HDA' produced by pressure-induced amorphization at liquid nitrogen temperature and below represents a limiting form of HDA and thus the phase spans a density interval between HDA' and VHDA. This procedure does not cover the part of the HDA spectrum that has a density below that of HDA' and can exist at $p = 0$ and $T = 80$ K in metastable form and therefore we do not

consider the imperfectly equilibrated HDA' to be a limiting form of HDA.

In Ref.[11] the interstitial occupancy in HDA' and VHDA at ambient pressure was calculated by integrating the O-O RDF between 2.3 and 3.3 Å. The values of 5.0 and 5.8 were found, respectively, corresponding to 50 % or almost 100 % occupancy of the "lynch pin location". It was speculated that due to some unknown specific mechanism only these values and no intermediate ones can be made stably at ambient pressure. We calculated the same occupancy at $T = 80$ K and $p = 0$ in our HDA' as well as in the RP decompressed from all pressures (Fig.11). In HDA' we found a value of 4.9 while in the HDA branch of decompressed RP we found an apparently continuous spectrum ranging from 4.3 (from 2.25 kbar) to about 6 (from pressures above 15 kbar). This again clearly shows that while VHDA indeed represents a limiting structure, this is not the case for HDA' whose occupancy close to the value of 5 can be regarded as accidental.

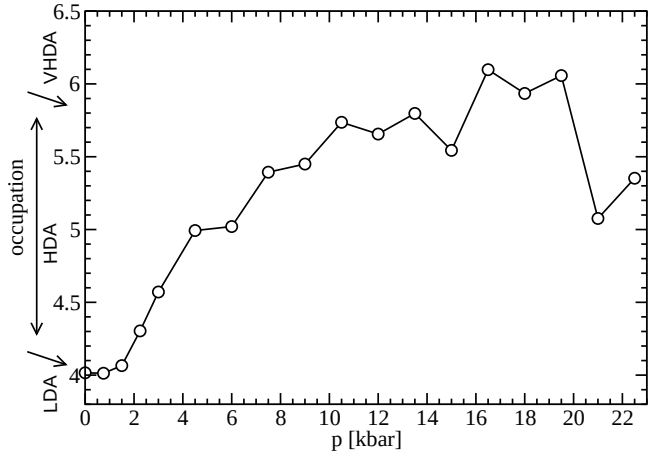

FIG. 11: Oxygen occupation number within 3.3 $\AA$ in the RP decompressed from pressure p at $T = 80$ K.

Recently, a neutron and X-ray diffraction study of the VHDA structure was reported in Ref.[17], showing the presence of at least seven well-defined shells in the RDF of the VHDA, extending almost to the distance of ~ 20 Å. This reveals the presence of an enhanced medium-range order in the VHDA. In order to check this property, we also prepared a bigger VHDA sample consisting of 2880 water molecules, allowing us to calculate the RDF up to a distance of 20 Å. We followed basically the same protocol as for the 360-molecule sample and annealed the HDA' at $p = 15$ kbar, but using shorter simulation times. The radial distribution function $D_{OO}(r) = 4\pi\rho r(g(r) - 1)$ in the decompressed sample is shown in Fig.12. Apart from the height of the first peak, our result agrees well with the experimental one (Fig.2(b)) in Ref.[17], and also shows at least seven coordination shells extending beyond ~ 16 Å. The presence of such enhanced medium-range order is likely to be related to the fact that the network topology of VHDA is dominated by large rings. In Ref.[17] the existence of a well-defined shell at 5 Å was pointed out; this is also clearly present in our RDF and in subsection III C we have identified its origin in the contribution of 9-membered rings (see Fig.7(b)).

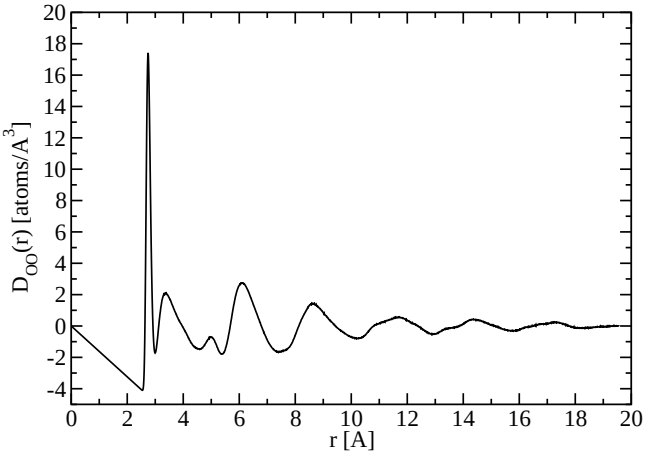

FIG. 12: Oxygen-oxygen radial distribution function $D_{OO}(r)$ for the VHDA prepared by annealing at $p = 15$ kbar and decompressing to zero pressure.

IV. ANALOGY TO SILICA

In spite of the different nature of the bonds between water molecules in amorphous ice and between silicon and oxygen atoms in amorphous silica, both systems consist of a continuous random network of corner-sharing tetrahedra[51] and in some windows of their phase diagrams display analogous phenomenologies when pressure is applied. Each tetrahedral unit in silica is made of a four-fold coordinated silicon atom in the center and four bridging oxygen atoms at the corners. The size distribution of the primitive rings[44,52] is peaked at six silicon atoms per ring and presents a sizable amount of four to ten-fold rings[42,44,52]. A high-density (HD) phase of amorphous silica was discovered by Grimsditch[53] about 20 years ago. It was shown that upon compression above 8 GPa a-SiO_2 undergoes a permanent densification which amounts to about 20% when the system is released to ambient pressure and the transition to the HD phase is accompanied by irreversible structural changes, observable by Brillouin and Raman measurement[53,54].

As in the case of amorphous ice, the nature of the phase transition is still debated, since no discontinuous volume change is observed in compression experiments[53,54,55] while computer simulations do not clarify whether there is a kinetically hindered first order transition[56] or a pressure window where there is a balance between two densification mechanisms[42,57]. In fact three different microscopic mechanisms cooperate in accommodating the amorphous silica network in a smaller volume[42,57,58,59] and make the phase transition between LDA and HDA apparently smoother than in amorphous ice. In the low pressure regime ($\simeq$3 GPa according to Refs.[42,57]) the

volume diminishes only by the buckling of the network, which results in a shift toward smaller values of the Si-O-Si bond angle distribution. In this process the tetrahedral units are not deformed and no bonds are broken. At higher pressures the buckling mechanism is supplemented by a substantial rebonding in the network, which mainly affects the medium-range order features: the local tetrahedral order is preserved but the ring-size distribution broadens and its peak shifts to larger rings[59]. In the response of silica to pressure the buckling and the rebonding mechanisms correspond to elastic and plastic regimes, respectively, as observed by Dávila *et al.* in MD simulations[43]. On the other hand, in both regimes short-range structural properties such as the Si-O-Si and the O-Si-O angles vary continuously. In addition, coordination defects may be formed and contribute to densification at even higher pressures (e.g. > 5 GPa in Ref.[42]). In ice the nature of the hydrogen bond inhibits this latter mechanism, as no more than four hydrogen bonds per water molecule can be formed: in fact the average coordination number of the RP is $\sim$4 at all the explored pressures. Consequently, when the limit for the topological densification is reached, amorphous ice turns back to an elastic regime (VHDA).

The increasing of the characteristic size of the rings upon densification is a general feature of both amorphous[52,60,61] and crystalline[62] tetrahedral networks. Among the tetrahedrally coordinated crystalline silica polymorphs, the lower density forms (cristobalite and tridimite) consist of six-membered rings only. In the denser silica crystals the average size of the rings increases accordingly to the density. For example coesite, which is 30% denser than α-cristobalite has an average ring size of ten and contains rings of size up to twelve. It is worth noting that unlike the HD crystalline phases of ice, it is impossible to form silica polymorphs with interpenetrating networks, because of sterical interactions.

V. CONCLUSIONS

Upon increase of pressure, relaxed amorphous ice undergoes a pronounced change of structure, from LDA at $p = 0$ to VHDA at $p > 10$ kbar. During this transformation, there is possibly a discontinuity between LDA and HDA, although from our simulations performed on a relatively small system we cannot distinguish between a weak first-order transition and a continuous change. Nevertheless, we can clearly distinguish the LDA and HDA regimes. This identification is based on the existence of a transition region characterized by a rapid change of density, on the presence of interstitial molecules and the behavior of the ring statistics. It is important to note that the main part of the overall change of the network topology does not occur during the LDA-HDA transition (similar conclusion was also made in Ref.[13]) but rather within the HDA phase, between $p \sim 2$ and 10 kbar. Concerning the as-prepared HDA', initially believed to be the only possible form of HDA, it does not seem to have any special importance and represents just one particular structure within the HDA megabasin. It is not in equilibrium even within the space of amorphous structures and its properties are determined by the conditions of preparation[28]. As shown above, when prepared at $T = 80$ K, HDA' is rather close to RP at 4.5 kbar. The HDA megabasin includes a broad range of structures with different local and medium-range order and also spans a broad interval of densities. On the high-density side, the onset of the VHDA regime marks the limit to which the densification can be pushed by adapting the network topology, without creating interpenetrating networks. The low density limit of HDA stability is more difficult to assess with precision. However, as shown experimentally by Refs.[12],[15],[13] and also in our simulations, the HDA region reaches substantially below HDA' density.

From the above it is clear that many forms of HDA exist and are metastable at $T = 80$ K upon decompression to $p = 0$. The important question then is, to what extent does this affect the use of the LDA/HDA phenomenology as support for the conjecture for the second critical point in water. In Ref.[16] it is claimed that since no unique HDA exists, it is difficult to justify the conjecture of a second critical point for water. We do not actually think that this is necessarily the case. In our picture, the variety of HDA ices which exist as metastable forms at $p = 0$ corresponds to the variety of topologically different HDL at different pressures. These various HDA forms cannot interconvert upon decompression at $T = 80$ K because this would involve rebonding and require overcoming free energy barriers. In Ref.[29] it was suggested that VHDA is a better candidate for the glassy phase continuous with the HDL, rather than HDA'. Since we reserve the use of VHDA for the particular high-pressure regime, we can say that all forms of the HDA branch of the RP appear to be equally good candidates for the glassy phase that is the putative continuation of the HDL. Consequently, the large density variation of HDA ice at $p = 0$ might reflect the existence of a region of high compressibility of the supercooled HDL just below the critical point[25]. As suggested in Refs.[13],[26], various forms of LDA ice may also exist at $T = 80$ K and $p = 0$, but their density variation is likely to be much smaller. A sharp transition may well exist between the upper limit of LDA and lower limit of HDA continua, as suggested by the experiments in Ref.[13]. To shed more light on this issue, simulations on larger systems combined with finite-size scaling techniques, as well as free energy calculations could be helpful.

In the discussion of the polyamorphism of ice its analogy with the properties of silica glasses can be useful, although attention should also be paid to important differences.

We should like to acknowledge stimulating discussions with V. Buch, D. Chandler, D. D. Klug, M. M. Koza and J. S. Tse.

* Permanent address: Department of Physics (FEI), Slovak University of Technology, Ilkovičova 3, 812 19 Bratislava, Slovakia; Electronic address: martonak@phys.chem.ethz.ch

[1] O. Mishima, L. D. Calvert, and E. Whalley, Nature (London) **310**, 393 (1984).
[2] O. Mishima, L. D. Calvert, and E. Whalley, Nature (London) **314**, 76 (1985).
[3] O. Mishima, J. Chem. Phys. **100**, 5910 (1994).
[4] P. H. Poole, F. Sciortino, U. Essmann, and H. E. Stanley, Nature **360**, 324 (1992).
[5] H. Tanaka, Nature **380**, 328 (1996).
[6] H. Tanaka, J. Chem. Phys. **105**, 5099 (1996).
[7] R. C. Dougherty, Chem. Phys. **298**, 307 (2004).
[8] P. H. Poole, U. Essmann, F. Sciortino, and H. E. Stanley, Phys. Rev. E **48**, 4605 (1993).
[9] T. Loerting, C. Salzmann, I. Kohl, E. Mayer, and A. Hallbrucker, Phys. Chem. Chem. Phys. **3**, 5355 (2001).
[10] S. Klotz, G. Hamel, J. S. Loveday, R. J. Nelmes, M. Guthrie, and A. K. Soper, Phys. Rev. Lett. **89**, 285502 (2002).
[11] J. L. Finney, D. T. Bowron, A. K. Soper, T. Loerting, E. Mayer, and A. Hallbrucker, Phys. Rev. Lett. **89**, 205503 (2002).
[12] C. A. Tulk, C. J. Benmore, J. Urquidi, D. D. Klug, J. Neuefeind, B. Tomberli, and P. A. Egelstaff, Science **297**, 1320 (2002).
[13] M. M. Koza, H. Schober, H. E. Fischer, T. Hansen, and F. Fujara, J. Phys.: Condens. Matter **15**, 321 (2003).
[14] M. Guthrie, J. Urquidi, C. A. Tulk, C. J. Benmore, D. D. Klug, and J. Neuefeind, Phys. Rev. B **68**, 184110 (2003).
[15] O. Mishima and Y. Suzuki, Nature **419**, 599 (2002).
[16] G. Johari and O. Andersson, J. Chem. Phys. **120**, 6207 (2004).
[17] M. Guthrie, C. A. Tulk, C. J. Benmore, and D. D. Klug, Chem. Phys. Lett. **397**, 335 (2004).
[18] D. D. Klug, Nature **420**, 749 (2002).
[19] A. K. Soper, Science **297**, 1288 (2002).
[20] P. Debenedetti and H. Stanley, Phys. Today **56**, 40 (2003).
[21] P. Debenedetti, J. Phys.: Condens. Matter **15**, R1669 (2003).
[22] C. Angell, Annu. Rev. Phys. Chem. **55**, 559 (2004).
[23] J. S. Tse and M. L. Klein, Phys. Rev. Lett. **58**, 1672 (1987).
[24] I. Okabe, H. Tanaka, and K. Nakanishi, Phys. Rev. E **53**, 2638 (1996).
[25] M. Yamada, H. E. Stanley, and F. Sciortino, Phys. Rev. E **67**, 010202(R) (2003).
[26] N. Giovambattista, H. E. Stanley, and F. Sciortino, Phys. Rev. Lett. **91**, 115504 (2003).
[27] I. Brovchenko, A. Geiger, and A. Oleinikova, J. Chem. Phys. **118**, 9473 (2003).
[28] B. Guillot and Y. Guissani, J. Chem. Phys. **119**, 11740 (2003).
[29] N. Giovambattista, H. E. Stanley, and F. Sciortino (2004), cond-mat/0403365 preprint.
[30] C. McBride, C. Vega, E. Sanz, and J. L. F. Abascal, J. Chem. Phys. **121**, 11907 (2004).
[31] R. Martoňák, D. Donadio, and M. Parrinello, Phys. Rev. Lett. **92**, 225702 (2004).
[32] E. Lindahl, B. Hess, and D. van der Spoel, J. Mol. Mod. **7**, 306 (2001).
[33] M. Parrinello and A. Rahman, Phys. Rev. Lett. **45**, 1196 (1980).
[34] H. J. C. Berendsen, J. P. M. Postma, W. F. van Gunsteren, A. DiNola, and J. R. Haak, J. Chem. Phys. **81**, 3684 (1984).
[35] U. Essmann, L. Perera, M. L. Berkowitz, T. Darden, H. Lee, and L. G. Pedersen, J. Chem. Phys. **103**, 8577 (1995).
[36] V. Buch, P. Sandler, and J. Sadlej, J. Phys. Chem. B **102**, 8641 (1998).
[37] W. L. Jorgensen, J. Chandrasekhar, J. D. Madura, R. W. Impey, and M. L. Klein, J. Chem. Phys. **79**, 926 (1983).
[38] E. Sanz, C. Vega, J. L. F. Abascal, and L. G. MacDowell, Phys. Rev. Lett. **92**, 255701 (2004).
[39] H. Tanaka, J. Chem. Phys. **113**, 11202 (2000).
[40] S. Klotz, G. Hamel, J. Loveday, R. Nelmes, and M. Guthrie, Z. Kristallogr. **218**, 117 (2003).
[41] O. Mishima and H. E. Stanley, Nature (London) **396**, 329 (1998).
[42] K. Trachenko and M. T. Dove, Phys. Rev. B **67**, 064107 (2003).
[43] L. P. Dávila, M.-J. Caturla, A. Kubota, B. Sadigh, T. D. de la Rubia, J. F. Shackelford, S. H. Risbud, and S. H. Garofalini, Phys. Rev. Lett. **91**, 205501 (2003).
[44] X. L. Yuan and A. N. Cormack, Comp. Mat. Sci. **24**, 343 (2002).
[45] P. Raiteri, A. Laio, and M. Parrinello, Phys. Rev. Lett. **93**, 87801 (2004).
[46] J. L. Finney, A. Hallbrucker, I. Kohl, A. K. Soper, and D. T. Bowron, Phys. Rev. Lett. **88**, 225503 (2002).
[47] A. K. Soper, Chem. Phys. **202**, 295 (1996).
[48] A. M. Saitta, T. Strässle, G. Rousse, G. Hamel, S. Klotz, R. J. Nelmes, and J. S. Loveday, J. Chem. Phys. **121**, 8430 (2004).
[49] N. B. Wilding, J. Phys.: Condens. Matter **9**, 585 (1997).
[50] J. S. van Duijneveldt and D. Frenkel, J. Chem. Phys. **96**, 4655 (1992).
[51] W. H. Zachariasen, J. Amer. Chem. Soc. **54**, 3841 (1932).
[52] C. S. Marians and L. W. Hobbs, J. non-Cryst. Solids **119**, 269 (1990).
[53] M. Grimsditch, Phys. Rev. Lett. **52**, 2379 (1984).
[54] R. J. Hemley, H. K. Mao, P. M. Bell, and B. O. Mysen, Phys. Rev. Lett. **57**, 747 (1986).
[55] Q. Williams and R. Jeanloz, Science **239**, 902 (1988).
[56] D. Lacks, Phys. Rev. Lett. **84**, 4629 (2000).
[57] K. Trachenko and M. T. Dove, Phys. Rev. B **67**, 212203 (2003).
[58] L. Huang and J. Kieffer, Phys. Rev. B **69**, 224203 (2004).
[59] L. Huang and J. Kieffer, Phys. Rev. B **69**, 224204 (2004).
[60] L. Stixrude and M. S. T. Bukowinski, Phys. Rev. B **44**, 2523 (1991).
[61] M. Grimsditch, A. Polian, and A. C. Wright, Phys. Rev. B **54**, 152 (1996).
[62] C. S. Marians and L. W. Hobbs, J. Non-Cryst. Solids **124**, 242 (1990).